3D Security Labels: Photostable Multi-material Multilayered QR Codes via Two-Photon Lithography

May Maung Zaw[1], Peiyuan Cao[2], Ray Guan Kit Ong[3], Darren Chi Jin Neo[4], Chee Leng Lay[1*].

1. I*nstitute of Materials Research and Engineering, Agency for Science, Technology and Research (A*STAR), 2 Fusionopolis Way, Innovis, 08-03, 138634 Singapore*
2. *Anglo-Chinese Junior College, 25 Dover Close East,139745 Singapore*
3. *Raffles Institution, One Raffles Institution Lane (along Bishan St 21), 575954 Singapore*
4. *KLA Corporation, 23 Serangoon North Avenue 5, 01-01 BTC Center, 554530*

*Email: lay_chee_leng@imre.a-star.edu.sg

KEYWORDS. 3D Security Labels, Multi-material Multilayered QR Codes, Two-Photon Lithography, Perylene Dyes

ABSTRACT: Current 3D micron-sized covert security labels are limited to simple designs involving graphics, texts, and numerical elements that constrain coding/decoding complexity and data density. Herein, we introduce photostable perylene dye-doped 3D security labels that feature intricate multi-material and multilayered machine-readable quick response (QR) codes fabricated using two-photon lithography (TPL). Leveraging precise label sizing and positioning, our innovative "QR codes-in-QR code" approach significantly enhances data storage capacity by over 250 %. To bolster security, we employ a 2.0 μm-thick 3D cover engraved with QR codes to conceal the 2D QR codes. We extend our advancements by introducing QR code-engraved 3D covers with stair-step patterns and novel 3D security labels featuring multi-material, multilayered machine-decipherable QR codes. These 3D QR code-based security labels demonstrate minimal color and information interference and offer exceptional security levels. Even after 6 months of storage, they consistently provide repetitive readouts without photobleaching. These labels augment data concealment, decoding complexity, and photostability in enhancing their efficacy and longevity in data storage, communication, and anti-counterfeiting applications.

1. INTRODUCTION

Counterfeit products are prevalent in many industries, causing economic damage, violating IPs, and endangering public health. In response to the escalating proliferation of counterfeit goods, advanced anti-counterfeiting technologies have been deployed to verify product authenticity. These technologies fall into two main categories. The first category includes overt labels like watermarks, barcodes, and holograms [1,2], which can be easily verified by simple observation. The second category comprises covert identifiers, such as color-tunable fluorescent security tags [3-7], molecular identification [8-10] and optical physical unclonable functions (PUFs) [11-13], which require specialized equipment or/and a database for verification. While overt labels offer expeditious and facile authentication, their conspicuous visibility renders them more susceptible to replication in contrast to covert labels. Covert labels, on the other hand, are invisible under the naked eye due to their micro-size and the material properties that conceal them under white light illumination [14-16]. Among these concealed technologies, three-dimensional (3D) security tags [8,9,12,17-20] possess greater data storage capacity and enhanced layers of security compared to their two-dimensional (2D) counterparts [10,11,21,22]. These 3D security tags are often made via photopolymerization-based 3D printing, with a growing interest in two-photon lithography (TPL) for anti-counterfeiting due to its non-linear two-photon absorption [23]. This characteristic empowers the creation of labels featuring sub-micrometer scale security attributes and extensive data-encoding potential.

Using TPL 3D graphical security labels based on surface-enhanced resonance scattering (SERS) have been fabricated [8,9]. Although the SERS-based 3D security labels allow the use of molecular fingerprints and height-dependent Raman hyperspectral images, the density of the encoded information is restricted to the aspect ratio and printed density of the candle-like microstructures, as well as the number of adsorbed chemical probes. To enhance data storage capacity and level of obscurity, 3D multilayered security tags incorporated with quantum dots (QDs) have been fabricated via TPL, with examples including an invisible carbon-dot doped luminescent single quick-response (QR) code concealed by a non-emissive layer [18], a 3D fluorescent graphics [19], and a 3D cross-grid design with height-dependent numerical patterns [20]. These studies primarily utilized QDs to impart fluorescent properties to the fabricated security labels. While QDs exhibit remarkable attributes like strong color purity, tunability, and long fluorescence lifetime, disadvantages exist due to concerns about cytotoxicity, thermochemical instability-induced QD degradation, and the tendency for QDs to aggregate and precipitate in solvents. These issues present suboptimal conditions for their application in photoresist formulation [24-26]. In contrast to QDs, a broad spectrum of commercially available organic dyes boasts biocompatibility and is commonly employed in biomedical applications [27], offering high solubility in organic solvents [28,29]. Nevertheless, prevalent drawbacks of most organic dyes used in the optical context involve issues of photostability and photobleaching [24,30]. Within the realm of organic dyes, perylene dyes derived from polycyclic aromatic hydrocarbons stand out due to their exceptional photostability, robust fluorescence output, thermal resilience, and resistance to environmental factors [31-33]. Notably, the integration of perylene dye-doped

photoresists into the domain of TPL-based 3D micro-/nanofabrication has not been unexplored.

Here, we demonstrate the TPL-assisted fabrication of 3D security labels doped with perylene dyes that incorporate intricate multi-material and multilayered machine-readable QR codes. Notably, the distinctive molecular structures of perylene dyes imbue these QR codes with unique fluorescent properties and photostability, resulting in 3D security labels that exhibit minimal information interference and exceptional photostability. By precise control over the label's size and spatial positioning, we strategically embed four perylene-doped QR codes within a 2D QR code. This is made possible by outstanding resolution afforded by TPL. Our "QR codes-in-QR code" approach substantially increases data storage capacity by ≥ 250 %. To make deciphering the code more complex, we locate a 3D engraved QR code cover featuring a stair-step pattern over the 2D QR codes. With a thickness of merely 2.0 μm, the 3D engraved QR code cover effectively protects and conceals the embedded 2D QR codes under standard optical conditions and fluorescence irradiation. Most significantly, our accomplishment in generating 3D QR code-based security labels, comprising four stacked layers of engraved QR codes using various perylene dyes, signifies a substantial leap in anti-counterfeiting innovation and capability. There is also no color and signal interference. Our innovative 3D QR code-based security label designs and fabrication approach have the potential to enhance decoding complexity and strengthen data concealment capabilities for data storage and anti-counterfeiting purposes, while ensuring machine readability and durability.

2. EXPERIMENTAL METHODS

Materials. Perylene dyes (fluorescent red and yellow) were supplied by Kremer Pigmente. IPL 780 photoresist was purchased from Nanoscribe GmbH & Co. KG. Isobornyl acrylate (IBOA, 98.5%), 1-methyl-2-pyrrolidinone (NMP, 99.5%) and (3-aminopropyl) triethoxysilane (APTES, 98%) were purchased from Sigma-Aldrich. Isopropyl alcohol (IPA, tech grade, 99%) was purchased from Aik Moh (Singapore). Deionized water (DI water) (18.0 MΩ·cm) was purified with a PURELAB Option Q ultrapure water system. All chemicals were used as received.

Formulation of fluorescent photoresists. Perylene red (PR) powder was mixed with IBOA monomer solution and IPL 780 with the concentration of PR powder at 1.0 g/L. For perylene yellow (PY)-doped photoresist, the concentration of PY in the final photoresist solution is 1.5 g/L.

Functionalization of glass substrates. Glass coverslips (22 μm × 22 μm) were treated with ozone plasma for 120 s on both surfaces of 22 μm × 22 μm glass coverslips inside a Triple-P Ozone Plasma chamber. The plasma-treated glass coverslips were immediately immersed in APTES solution (1 vol%) for 5 min, followed by 2 min washing in ethanol/water (1:1 vol ratio). They were subsequently rinsed with DI water to remove any excess APTES, and the glass substrate was dried under a flow of nitrogen gas. The glass coverslips were then placed in the oven set at 70 °C for drying

Structural design and fabrication method. SolidWorks (version 2021) and SketchUp Pro Desktop computer-aided design (CAD) software were used to prepare stereolithography (STL) files for 3D printing. The QR codes were generated using an online QR code generator (https://www.qrcode-tiger.com/). Each QR code comprises a data-encoded region alongside non-data encoded elements, including finder, alignment, and timing patterns (Figure S1). These patterns are essential for the detection and readability of the label. Additionally, the data encoding process of a QR code integrates the universe Reed-Solomon error correction mechanism [34]. A NanoScribe Photonic Professional GT (NanoScribe) (equipped with a fiber-couple diode laser at a wavelength of 780 nm, pulse frequency of 80 MHz and pulse duration of 120 fs) was used to fabricate the 2D/3D QR codes. An oil-immersion Plan-Apochromat objective lens (63 ×, NA=1.4, WD = 190 μm) was employed for laser beam focusing. 2D/3D QR codes were fabricated on APTES-functionalized glass substrates by scanning the laser beam layer by layer using a galvo-scanner (for X-Y directions) and a piezo stage (Z direction). The optimum processing parameters—laser power (LP) and laser scanning speed (SS) for the microfabrication of 2D/3D QR codes are given in Figure S2. For resist development, the substrates were rinsed in NMP for 10 min, followed by immersion in IPA for 15 min to wash away residual resin. The NanoScribe navigation system was used for accurate spatial positioning for multilayered and multi-material fabrication. Our fabrication workflow for the multi-material QR codes is briefly outlined in Figure 2.

Characterization. For PR and PY material characterization, UV-Vis absorption spectra were measured using a Shimadzu UV-1800 double-beam spectrophotometer, and fluorescence emission spectra were obtained using a Shimadzu RF-5301PC spectrofluorophotometer. Fourier-transform infrared spectroscopy (FTIR) spectra of the materials were obtained using a nanoscale infrared (nanoIR) spectrometer (Anasys NanoIR 2, Bruker) with contact mode. Fluorescence and bright field images of 3D-printed structures were captured using an Olympus BX51 fluorescence microscope with 100× objective lens (NA = 0.8) and under blue and green illumination for fluorescence. Confocal images and time-based fluorescence intensity spectra were obtained on a Leica Stellaris 8 Falcon (Inverted) confocal microscope with 63× oil immersion objective lens (NA = 1.4). The Leica Stellaris confocal system is equipped with a tunable white light laser and for our application, we used 470 nm and 550 nm excitation wavelengths. Topographical characterization of the 3D-printed structures was carried out on a scanning electron microscope (FESEM JEOL JSM-7600F) with an accelerating voltage of 15 kV, after sputtering with gold (Cressington 108 Sputter Coater, 30 mA, 35 s coating time). Surface profiler (Tencor P16) using a scan speed of 10 μm/s and contact force of 0.5 mN. Transmittance measurements of the printed covers were conducted on a UV-Vis-NIR microspectrophotometer (CRAIC 508 PVTM) using 10× objective lens (NA = 0.45) and clean glass substrate as the reference.

3. RESULTS AND DISCUSSION

3.1 Properties and stability of fluorescent dyes. Long-term photostability and machine-readability are essential attributes for the durability and reliability of security labels when used in real-world conditions. To construct security labels with extended optical lifetimes for repetitive

scanning and decoding, we opt for perylene red (PR) and perylene yellow (PY) dyes in our acrylate-resist formulations (Figure 1). We make this choice based on their outstanding photostability [29-31] and their optical compatibility and miscibility with our acrylate photoresist. Our TPL system has an excitation wavelength of 780 nm with an effective photoinitiator absorption band at 390 nm. Notably, both PR and PY exhibit insignificant absorbance at λ = 390 nm and 780 nm (Figure 1A and 1B, Figure S3). PR's absorbance peaks are observed at λ = 226 nm, 284 nm, 445 nm, and 580 nm (Figure 1A); whereas PY's absorbance peaks fall at λ = 217 nm, 259 nm, 443 nm, and 470 nm (Figure 1B). This allows unhindered two-photon absorption of the photoinitiator molecules in the acrylate photoresist to initiate two-photon polymerization (TPP) [23]. Additionally, when excited by a green laser (λ_{ex} = 550 nm), only PR emits red fluorescence peaking at λ » 600 nm (Figure 1A, Figure S3). On the other hand, upon exposure to a blue laser (λ_{ex} = 450 nm), PY displays green fluorescence with a fluorescence peak at λ » 490 nm (Figure 1, Figure S3). The difference in absorbance and fluorescence spectra of PRs and PYs in the UV-visible region validate their compatibility in acrylate-based photoresist formulations, establishing their suitability for multi-color security label fabrication.

To assess the photostability of PR- and PY-doped microfabricated 2D QR codes following TPP and repetitive laser scanning for decoding, we subject the microfabricated 2D QR codes to alternating exposure cycles of prolonged white light and laser illumination (Figure 1D and 1E). Throughout this process, we monitor and measure their fluorescence intensities at regular intervals, with a confocal microscopy system. For each measurement cycle, PR- and PY-doped 2D QR codes were exposed to laser light for 1.5 min (under λ_{ex} = 550 nm, detection range 560 nm – 743 nm) and 2 min (under λ_{ex} = 470 nm, detection range 480 nm – 693 nm) respectively, which was then followed by 15-min exposure to microscope white light of intensity ≥ 407 μW. Both PR- and PY-doped 2D QR codes exhibit remarkable stability in fluorescence intensities (Figure 1D and 1E, Figure S4), demonstrating their exceptional photostability after TPP and 60 min of intense white light and blue/green light exposure. The slight fluctuations in measured fluorescence intensities observed during the photostability studies can be attributed to a minor focus drift of the confocal microscope that occurred during the experiment (Figure 1D and 1E). It is crucial to emphasize that the tested 2D QR codes retain their vibrant fluorescence and machine-readability upon re-excitation, exhibiting no signs of fluorescence quenching, even after six months of storage in dark ambient conditions (25 °C, ~ 75 % RH) (Figure S5B). In addition to optical verifications, chemical analysis via FTIR also confirms the presence of perylene dye molecules within the microfabricated 2D QR codes (Figure S6). On this note, their robust photostability makes perylene dyes an ideal choice for 3D-microfabricating durable and machine-readable security labels that meet the fundamental demands of real-world applications.

3.2 Enhanced data capacity of 2D QR codes via QR codes-in-QR code design. Next, we leveraged the contrasting optical properties of pristine acrylate photoresist and PR-doped acrylate photoresist to create a 2D security label featuring a QR codes-in-QR code design (Figure 2A, 2B). The dual-material security label with the QR codes-in-QR code design is constructed via accurate size control and precise spatial positioning to embed four smaller PR-doped QR codes (~ 22 μm × 22 μm) into a base pristine acrylate QR code (250 μm × 250 μm) (Figure 2). PR-doped QR codes 1, 2 and 4 are printed inside the finder patterns, while the PR-doped QR code labeled 3 is embedded within the data-encoded region of the main pristine acrylate QR code (Figure 2A and 2B, Figure S5). Under blue light illumination (λ_{ex} ≈ 450 nm), five machine-readable QR codes become apparent, each leading to its respective website upon scanning (Figure 2B and Figure S5A). However, when exposed to green light (λ_{ex} ≈ 550 nm), only the four PR-doped QR codes are activated (Figure S5A). This observation emphasizes that all QR codes are constructed with well-defined modules, ensuring that there is no color or information crosstalk. Additionally, due to their excitation wavelength-specific optical properties, it necessitates knowledge of the wavelength information to gain access to these fluorescent QR codes, adding an additional layer of security.

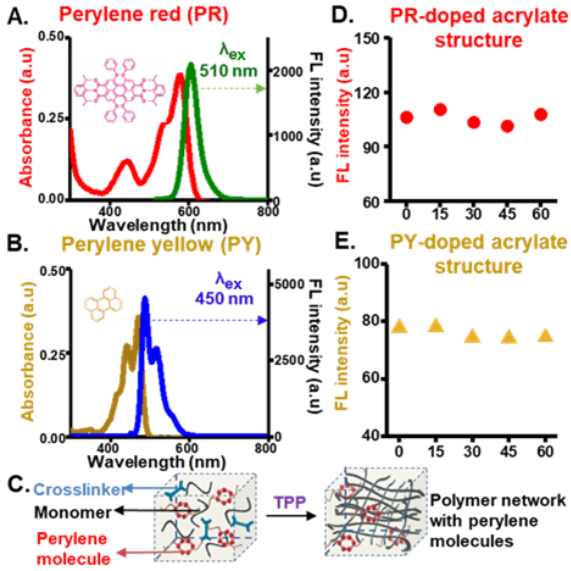

Figure 1. Optical properties of perylene red (PR) and perylene yellow (PY). (A) Depiction UV-Vis absorbance and fluorescence spectra for PR. (B) Depiction of UV-Vis absorbance and fluorescence spectra for PY. (C) Schematic representation illustrating the integration of perylene dyes into crosslinked acrylate polymeric structures through two-photon polymerization (TPP). (D) Monitoring of the fluorescence stability of microfabricated PR-doped acrylate structure over 1 hr with an excitation wavelength (λ_{ex}) of 550 nm. (E) Evaluation of the fluorescence stability of fabricated PY-doped acrylate structure over 1 hr with λ_{ex} = 470 nm.

Our method which involves substituting modules in the base QR code with four smaller PR-doped QR codes can be viewed as a form of data multiplexing [36]. This QR codes-in-QR code design enables us to enhance the data storage density (data capacity per unit area) of the base QR code without modifying its dimensions. The base pristine-acrylate QR code (version 5) has a data capacity of 864 bits; while the four embedded PR-doped QR codes have a combined data capacity of 1304 bits (QR codes 1 and 3 are version 3 with capacity = 2 × 440 bits = 880 bits, QR code 2 is version 1 with capacity = 152 bits, and QR code 4 is version

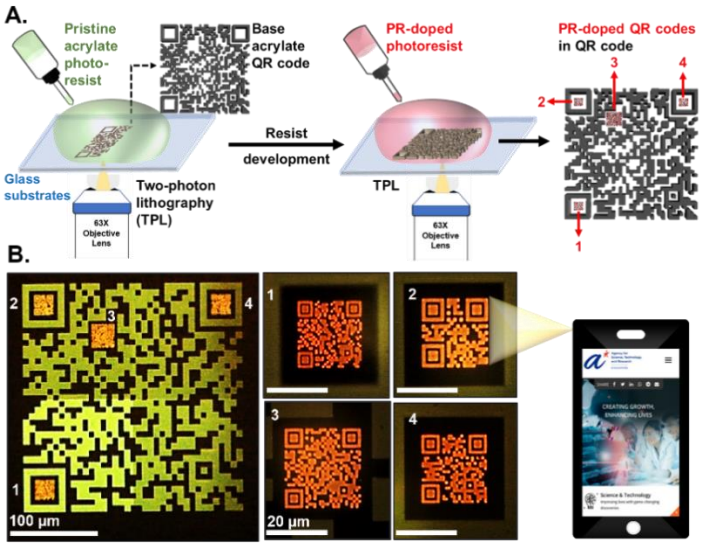

Figure 2. Fabrication workflow and printed dual-material QR code. (A) Fabrication workflow for dual-material QR codes-in-QR code anti-counterfeiting label. B) Machine-readable fluorescence images of QR codes under excitation λ_{ex} = 450 nm: 250 µm × 250 µm main QR code (version 5) redirects to https://www.a-star.edu.sg/imre/research-departments/nanofabrication and PR-doped QR code 1 (version 3) redirects to https://www.mti.gov.sg/, QR code 2 (version 1) redirects to https://www.a-star.edu.sg/, QR code 3 (version 3) redirects to https://www.a-star.edu.sg/imre/, QR code 4 (version 2) redirects to https://www.gov.sg/.

2 with capacity = 272 bits) [35]. By replacing modules in the base QR code with four smaller PR-doped QR codes, we achieve data multiplexing to enhance the data capacity of the base 2D QR code by 250 %, from an initial 864 bits to a total of 2168 bits. Considering this, our QR codes-in-QR code design notably contributes to enhancing data density and bolstering the security of advanced QR codes through data/information multiplexing.

3.3 3D Engraved Covers. To enhance the data capacity and security level of a security label, the transformation of a 2D security label into a 3D design has emerged as a promising approach [8,9,12,17-20]. We initiate the process by concealing a 2D PR-doped QR code with a flat-surfaced 3D cover. Research indicates that while a 2D fluorescent QR code can be masked by a 3D flat cover in bright-field observation with an optical microscope, the code remains visible under a fluorescence microscope [18]. However, increasing the thickness of the 3D flat cover from 1.5 µm to 15 µm does not improve its cloaking effect under fluorescence microscopy (Figure S8).

With this in mind, we engraved a QR code on the 3D cover to assess its influence on the transmittance and cloaking efficiency (Figure 3). Our findings reveal that the engraved cover (cover height, h = 7 µm; film thickness, t = 5 µm; engraved depth, t = 4 µm) exhibits a 50 % reduction in transmittance (~ 50 %) as compared to that (~ 100%) of the flat cover (cover height, h = 7 µm; film thickness, t = 5 µm) of the same thickness (Figure 3A, 3B, Figure S9). The observed reduction in transmittance is a consequence of the scattering and diffraction of light caused by the engraved cover. Consequently, in addition to being invisible under bright-field observation, the fluorescence image of the 2D QR code concealed beneath the 3D engraved cover is obscured by a hazy effect, rendering the 2D QR code indiscernible (Figure 3C).

This fluorescence haze effect necessitates the use of a confocal microscope to retrieve the encoded QR code underneath the engraved cover. Most notably, a 3D engraved cover with t = 2 µm suffices to disguise an embedded 2D QR code (Figure S11). Additionally, our observations indicate that the cloaking efficiency of the 3D engraved cover increases with an increase in film thickness (t) and engraved depth (d) (Figure S11A, S11B). Furthermore, to fabricate a 3D engraved cover with a QR code with well-defined features, the engraved depth (d) must adhere to the specified aspect ratio threshold of ≤ 6.4 (Figure S10B). Similarly, the film thickness (t) must satisfy the engraved depth (d) and aspect ratio requirements (Figure S10, S11). These findings provide us with the flexibility to design 3D engraved QR code-based covers with versatility.

To enhance the security level, we implement a stair-step design for a 3D engraved QR code cover (Figure 4). It is accomplished by dividing a 3D engraved QR code cover into three distinct regions with varying heights (Region 1, h = 4 µm; Region 2, h = 5.5 µm; and Region 3, h = 7 µm), each with their respective film thickness (Region 1, t = 2 µm; Region 2, t = 3.5 µm; and Region 3, t = 5 µm) and engraved depths (Region 1, d = 1.5 µm; Region 2, d = 3 µm; and Region 3, d = 4.5 µm) (Figure 4A and Figure S13). The observations in bright field mode reveal that the varying heights of the engraved QR code cover with stair-step design require different focal depths under an optical microscope, leading to partially blurred images at a single focal depth (Figure 4B).

Furthermore, confocal microscopy (λ_{ex} = 405 nm) also fails to render a clear QR code image from the engraved cover with a stair-step design for decoding (Figure 4C). Producing a machine-readable image of the engraved QR code cover with a stair-step design, requires the use of an SEM (Figure 4A). On the other hand, the concealed PY and PR-doped QR codes can only be unveiled and deciphered using a confocal microscope at λ_{ex} = 470 nm and λ_{ex} = 550 nm, respectively (Figure 4C). These findings underscore the innovative application of our stair-step design for the 3D

engraved QR code, which incorporates unique regions with differing heights, film thicknesses, and engraved depths, to enhance data capacity, complicate data retrieval, and improve security measures.

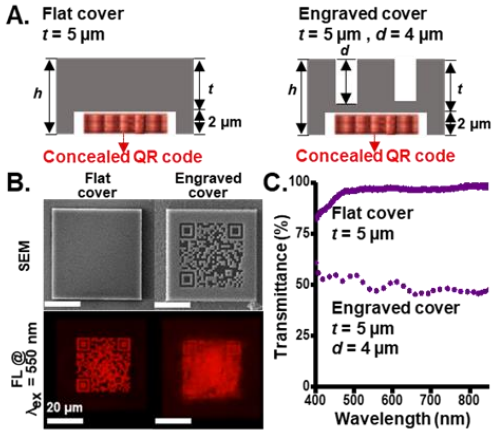

Figure 3. Effect of cover design on transmittance and cloaking efficiency. (A) Schematic illustrations showcase designs of the flat cover and engraved cover, with a QR code embedded underneath the covers. (B)(top) SEM micrographs of flat cover (thickness, t = 5 μm), and engraved cover (t = 5 μm; engraved depth, d = 4 μm). (Bottom) When conducting fluorescence imaging at λ_{ex} = 550 nm, the QR code embedded under the flat cover is completely revealed and can be read by a QR code scanner. However, the fluorescent image of the QR code embedded under the engraved cover is distorted and cannot be deciphered. (C) Comparison of transmittance between the flat cover and engraved cover as shown in (B).

3.4 Stacked-engraved cover design. To continue exploring 3D security labels that incorporate multi-material, multilayered machine-decipherable QR codes, we fabricate a 3D QR code-based security label with a quadruple-layer design. By utilizing TPP and our novel approach for generating 3D engraved QR codes, we successfully created a 3D security label comprising four layers of QR codes, each fabricated from distinct materials and each linked to different websites (Figure 5). The first layer comprises 2D PR- and PY-doped QR codes arranged in a check pattern and adhering to a glass substrate. The second layer showcases a 3D engraved QR code cover made from pristine acrylate photoresist. The third layer presents a 3D PR-doped engraved QR code, and the fourth and uppermost layer houses the 3D PY-doped engraved QR code (Figure 5A). Through images captured under bright-field illumination, fluorescence imaging and SEM, only the uppermost PY-doped engraved QR code is visible and decipherable (Figure 5B, SI Video 1).

To disclose the information within the 3D quadruple-layer security label, laser excitation at specific wavelengths is required to expose the underlying QR codes: λ_{ex} = 405 nm for the pristine acrylate layer, λ_{ex} = 470 nm for the PY-doped layers and λ_{ex} = 550 nm for the PR-doped layers (Figure 5C, SI Video 2). This limits data access exclusively to confocal imaging. We do not adopt the reported strategy on including blank structures made of pristine acrylate photoresist between neighboring fluorescent layers and structures to

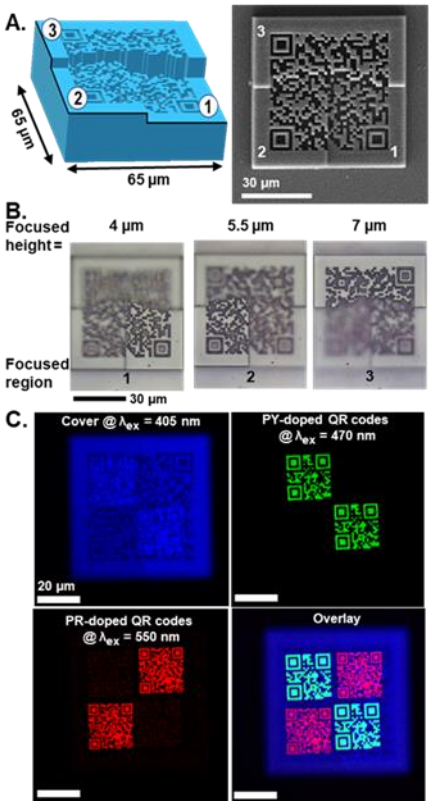

Figure 4. QR codes embedded beneath an 3D engraved QR code cover with a stair-step pattern. (A) Schematic diagram and SEM micrograph of the 3D engraved QR code cover with a stair-step pattern. (B) Observing different regions of the 3D stepped-engraved QR code cover at different focusing depth under bright-field illumination. Due to the stair-step design, the engraved QR code at the cover cannot be fully kept in focus and resolved by optical and fluorescence microscopy. (C) Successful visualization of the stepped-engraved QR code cover and the concealed PY- and PR-doped QR codes via confocal microscope. The 3D stepped-engraved QR code cover made of pristine acrylate photoresist (under λ_{ex} = 405 nm) links to (https://www.a-star.edu.sg/imre/research-departments/nanofabrication). For the 2D QR codes fabricated on the glass substrate, the green-fluorescent (under λ_{ex} = 470 nm) PY-doped QR codes redirect to (https://www.a-star.edu.sg/); while the red-fluorescent (under λ_{ex} = 550 nm) PR-doped QR codes redirect to (https://www.a-star.edu.sg/imre/).

prevent information crosstalk [19]. Through our multilayer multi-material stacking design, we achieve a 3D security label comprising four layers of QR codes with well-defined features and insignificant fluorescence crosstalk between layers and microstructures. Beyond the multi-layer data concealment strategy, our 3D stacked design amplifies data encoding capacity by a factor ≥ 5, allowing secure information to be encoded across multiple layers within a single printing space. Our 3D stacked quadruple-layer security label not only reinforces data security but also increases data capacity.

As a result, compared to 3D security labels designed with micro-graphics, numbers, and text [18-20], our 3D QR code-based security labels of similar size offer a significant

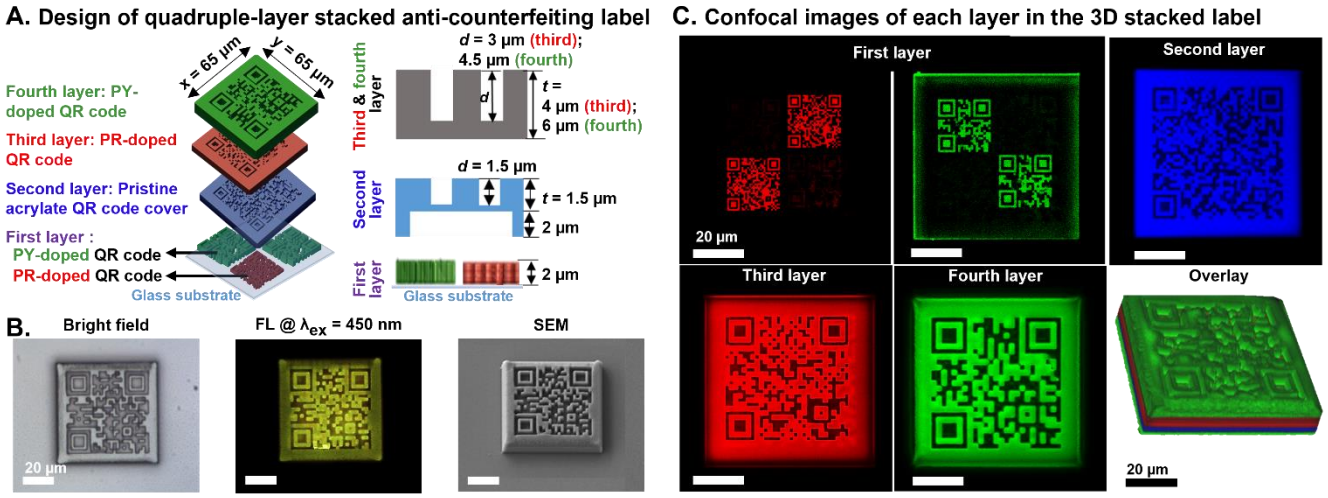

Figure 5. Quadruple-layer security label featuring stacked QR codes. (A) Schematic illustrations of a 3D security label incorporating four layers of QR codes. The first layer, affixed to a glass substrate, encompasses two QR codes doped with PY (hyperlinked to https://www.a-star.edu.sg/) and another pair doped with PR (linked to https://www.a-star.edu.sg/imre/). The second layer showcases a 3D engraved QR code cover associated with (https://www.a-star.edu.sg/imre/research-departments/nanofabrication) and it is made of the pristine acrylate photoresist. The third and fourth layers feature engraved QR codes doped with PR and PY, respectively, directing to (https://www.mti.gov.sg/) and (https://www.gov.sg/). (B) Optical images and SEM micrograph of the quadruple-layer security label. (C) Confocal images of the quadruple-layer 3D security label and its constituents: concealed 2D QR codes in the first layer and three layers of the predesigned engraved QR codes superimposed at varying heights. There is no information interference caused by color diffusion among modules within each engraved QR code, and likewise, there is no signal crosstalk between the stacked QR codes.

advantage due to their greater data storage capacity and enhanced functionality. This advantage arises from a QR code's capacity and flexibility to encode different types of data in a 2D matrix format, its ability to link to both internal and external databases, and its versatility in design and post-treatments [35,37].

4. CONCLUSION

In conclusion, we successfully microfabricated photostable perylene dye-incorporated security labels consisting of multi-material, multilayered machine-readable QR codes using TPL. Instead of microstructures with protruding designs in the conventional fabrication of security tags, we engrave QR codes into 3D films which enable versatile topological designs. Our engraving approach not only allows us to cloak the embedded 2D QR codes effectively, but also allows us to fabricate multi-material 3D security labels with four layers of machine-readable QR codes without any information interference. Furthermore, our QR codes-in-QR code design achieves ≥ 250 % increase in data capacity with data multiplexing. By employing our fabrication approach, combined with design information and data/color-multiplexing techniques, we can increase both data capacity and the complexity of decoding a security label in the future. By using fluorescent-based photoresist, we also have the option of adding another layer of security via spectral matching and resolving the different color modules. Besides anti-counterfeiting, our technique is also useful for high-density multi-dimensional optical storage and optical meta-waveguides.

ASSOCIATED CONTENT

Supporting Information

The Supporting Information is available free of charge at ACS Online.

Explanation on QR code structure, TPL parameter optimization test data, additional UV-Vis absorbance and fluorescence spectra, fluorescence intensity-over-time data, FTIR data, transmittance data, surface profiler data, additional SEM, and optical images.

Video 1: 3D view video of quadruple-layer 3D stacked QR codes.

Video 2: Mobile scanning to test machine-readability of QR codes in each layer of the 3D stacked quadruple-layer label as shown in Figure 5.

AUTHOR INFORMATION

Corresponding Author

*E-mail: lay_chee_leng@imre.a-star.edu.sg (Chee Leng Lay)

Authors

E-mail: may_maung_zaw@imre.a-star.edu.sg (May Maung Zaw)

E-mail: caopeiyuan040512@gmail.com (Peiyuan Cao)

E-mail: 23yongg911i@student.ri.edu.sg (Guan Kit Ray Ong)

E-mail: Darren.neo@kla.com (Darren Chi Jin Neo)

Author Contributions

The manuscript was written through the contributions of all authors. All authors have given approval to the final version of the manuscript.

Funding

The authors acknowledge financial support from the Science and Engineering Research Council (SERC), Agency of

Science Technology and Research (A*STAR) (A*STAR SERC MTC YIRG; grant number M21K3c0126).

Notes

The authors declare no competing financial interest.

ACKNOWLEDGMENTS

The authors thank Dr. Ma Xiaoxiao, Manager of A*STAR Microscopy Platform (AMP) for microscopy support; and Koh Xue Qi, Research Engineer at the Polymer Composite Department (PMC), Institute of Materials Research and Engineering (IMRE), for FTIR characterization support.

REFERENCES

(1) Bansal, D.; Malla, S.; Gudala, K.; Tiwari, P., Anti-Counterfeit Technologies: A Pharmaceutical Industry Perspective. *Scientia Pharmaceutica* **2013,** 81 (1), 1-13.

(2) Shah, R. Y., Prajapati, P. N., & Agrawal, Y. K. Anticounterfeit Packaging Technologies. *Journal of Advanced Pharmaceutical Technology & Research* **2010**, 1(4), 368–373.

(3) Przybylska, D., Grzyb, T., Erdman, A., Olejnik, K., & Szczeszak, A. Anti-Counterfeiting System based on Luminescent Varnish Enriched by NIR- excited Nanoparticles for Paper Security. *Scientific Reports* **2022**, 12(1), 19388.

(4) Suo, H., Zhu, Q., Zhang, X., Chen, B., Chen, J., & Wang, F. High-Security Anti-Counterfeiting through Upconversion Luminescence. *Materials Today Physics* **2021**, 21, 100520.

(5) Chen, X., Wang, Q., Wang, X.-J., Li, J., & Xu, G.-B. Synthesis, and Performance of ZnO Quantum Dots Water-based Fluorescent Ink for Anti-Counterfeiting Applications. *Scientific Reports* **2021**, 11(1), 5841.

(6) Yao, W., Lan, R., Li, K., & Zhang, L.. Multiple Anti-Counterfeiting Composite Film Based on Cholesteric Liquid Crystal and QD Materials. *ACS Applied Materials & Interfaces* **2021**, 13(1), 1424–1430.

(7) Liu, J., Zhuang, Y., Wang, L., Zhou, T., Hirosaki, N., & Xie, R.-J. Achieving Multicolor Long-Lived Luminescence in Dye-Encapsulated Metal–Organic Frameworks and Its Application to Anticounterfeiting Stamps. *ACS Applied Materials & Interfaces* **2018**, 10(2), 1802–1809.

(8) Liu, Y., Lee, Y. H., Lee, M. R., Yang, Y., & Ling, X. Y. Flexible Three-Dimensional Anticounterfeiting Plasmonic Security Labels: Utilizing Z-Axis-Dependent SERS Readouts to Encode Multilayered Molecular Information. *ACS Photonics* **2017**, 4(10), 2529–2536.

(9) Lay, C. L., Koh, C. S. L., Wang, J., Lee, Y. H., Jiang, R., Yang, Y., Yang, Z., Phang, I. Y., & Ling, X. Y. Aluminum Nanostructures with Strong Visible-Range SERS Activity for Versatile Micropatterning of Molecular Security Labels. *Nanoscale* **2018**, 10(2), 575–581.

(10) Zhou, Y., Zhao, G., Bian, J., Tian, X., Cheng, X., Wang, H., Chen, H. Multiplexed SERS Barcodes for Anti-Counterfeiting. *ACS Applied Materials & Interfaces* **2020,** 12 (25), 28532-28538.

(11) Liu, Y., Han, F., Li, F., Zhao, Y., Chen, M., Xu, Z., Zheng, X., Hu, H., Yao, J., Guo, T., Lin, W., Zheng, Y., You, B., Liu, P., Li, Y., & Qian, L. Inkjet-Printed Unclonable Quantum Dot Fluorescent Anti-Counterfeiting Labels with Artificial Intelligence Authentication. *Nature Communications* **2019**, 10(1), 2409.

(12) Zhang, J., Liu, Y., Njel, C., Ronneberger, S., Tarakina, N. V, & Loeffler, F. F. An All-In-One Nanoprinting Approach for the Synthesis of a Nanofilm Library for Unclonable Anti-Counterfeiting Applications. *Nature Nanotechnology* **2023**, 18, 1027–1035.

(13) Hu, Y. W., Zhang, T. P., Wang, C. F., Liu, K. K., Sun, Y., Li, L., Lv, C. F., Liang, Y. C., Jiao, F. H., Zhao, W. B., Dong, L., Shan, C. X. Flexible and Biocompatible Physical Unclonable Function Anti-Counterfeiting Label. *Advanced Functional Materials* **2021,** 31 (34).

(14) Chen, B.; Xie, H.; Wang, S.; Guo, Z.; Hu, Y.; Xie, H., UV Light-Tunable Fluorescent Inks and Polymer Hydrogel Films based on Carbon Nanodots and Lanthanide for Enhancing Anti-Counterfeiting. *Luminescence* **2019,** 34 (4), 437-443.

(15) Zuo, M.; Qian, W.; Li, T.; Hu, X. Y.; Jiang, J.; Wang, L., Full-Color Tunable Fluorescent and Chemiluminescent Supramolecular Nanoparticles for Anti-Counterfeiting Inks. *ACS Applied Materials & Interfaces* **2018,** 10 (45), 39214-39221.

(16) Zhao, H.; Qin, X.; Zhao, L.; Dong, S.; Gu, L.; Sun, W.; Wang, D.; Zheng, Y., Invisible Inks for Secrecy and Anticounterfeiting: From Single to Double-Encryption by Hydrochromic Molecules. *ACS Applied Materials & Interfaces* **2020,** 12 (7), 8952-8960.

(17) Meruga, J. M.; Cross, W. M.; Stanley May, P.; Luu, Q.; Crawford, G. A.; Kellar, J. J., Security Printing of Covert Quick Response Codes Using Upconverting Nanoparticle Inks. *Nanotechnology* **2012,** 23 (39).

(18) Jaiswal, A.; Rani, S.; Singh, G. P.; Saxena, S.; Shukla, S., Two-Photon Lithography of Fluorescence-Encoded Quick-Read Micro-Code for Anti-Counterfeiting Applications. *Journal of Physics: Photonics* **2021,** 3 (3).

(19) Peng, S.; Sun, S.; Zhu, Y.; Qiu, J.; Yang, H., Colorful 3D Anti-Counterfeiting Label Using Nanoscale Additive Manufacturing. *Virtual and Physical Prototyping* **2023,** 18 (1).

(20) Mayer, F.; Richter, S.; Hübner, P.; Jabbour, T.; Wegener, M., 3D Fluorescence-Based Security Features by 3D Laser Lithography. *Advanced Materials Technologies* **2017,** 2 (11).

(21) You, M., Zhong, J., Hong, Y., Duan, Z., Lin, M., & Xu, F. Inkjet Printing of Upconversion Nanoparticles for Anti-Counterfeit Applications. *Nanoscale* **2015**, 7(10), 4423–4431.

(22) Yao, W.; Tian, Q.; Liu, J.; Wu, Z.; Cui, S.; Ding, J.; Dai, Z.; Wu, W., Large-Scale Synthesis and Screen Printing of Upconversion Hexagonal-Phase $NaYF_4$: Yb^{3+}, $Tm^{3+}/Er^{3+}/Eu^{3+}$ Plates for Security Applications. *Journal of Materials Chemistry C* **2016,** 4 (26), 6327-6335.

(23) O'Halloran, S., Pandit, A., Heise, A., & Kellett, A. Two-Photon Polymerization: Fundamentals, Materials, and Chemical Modification Strategies. *Advanced Science* **2023**, 10(7), 1–18.

(24) Resch-Genger, U., Grabolle, M., Cavaliere-Jaricot, S., Nitschke, R., & Nann, T. Quantum Dots Versus Organic Dyes as Fluorescent Labels. *Nature Methods* **2008**, 5(9), 763–775.

(25) Issa, A., Ritacco, T., Ge, D., Broussier, A., Lio, G. E., Giocondo, M., Blaize, S., Nguyen, T. H., Dinh, X. Q., Couteau, C., Bachelot, R., & Jradi, S. Quantum Dot Transfer from the Organic Phase to Acrylic Monomers for the Controlled Integration of Single-Photon Sources by Photopolymerization. *ACS Applied Materials & Interfaces* **2023**, 15(21), 25819–25830.

(26) Ko, J., Jeong, B. G., Chang, J. H., Joung, J. F., Yoon, S.-Y., Lee, D. C., Park, S., Huh, J., Yang, H., Bae, W. K., Jang, S. G., & Bang, J. Chemically Resistant and Thermally Stable Quantum Dots prepared by Shell Encapsulation with Cross-

Linkable Block Copolymer Ligands. *NPG Asia Materials* **2020**, 12(1),19.
(27) Cheng, W., Chen, H., Liu, C., Ji, C., Ma, G., & Yin, M. Functional Organic dyes for Health-Related Applications. *View* **2020**, 1(4), 1–14.
(28) Qi, Y., Xie, R., Yu, A., Bukhari, M. N., Zhang, L., & Cao, C. Effect of Ethylene Glycol and its Derivatives on the Aggregation Properties of Reactive Orange 13 Dye. *RSC Advances* **2020**, 34373–34380.
(29) Kim, J. Y., Hwang, T. G., Kim, S. H., Namgoong, J. W., Kim, J. E., Sakong, C., Choi, J., Lee, W., & Kim, J. P. Synthesis of High-Soluble and Non-Fluorescent Perylene Derivatives and their Effect on the Contrast Ratio of LCD Color Filters. Dyes and Pigments. *Science Direct* **2017**, 136, 836–845.
(30) Fili N, Toseland CP. Fluorescence and Labelling: How to Choose and What to Do. *Experientia Supplementum* **2014**, 105, 1–24.
(31) Qian, G., Yang, Y., Wang, Z., Yang, C., Yang, Z., & Wang, M. Photostability of Perylene Orange, Perylene Red and Pyrromethene 567 Laser Dyes in Various Precursors Derived Gel Glasses. *Chemical Physics Letters* **2003**, 368(5), 555–560.
(32) Lewis, P. A. Colored Organic Pigments. In Applied Polymer Science:21st Century, *Science Direct* **2000**; pp 493-526.
(33) Avlasevich, Y., Li, C., & Müllen, K. Synthesis and Applications of Core-Enlarged Perylene Dyes. *Journal of Materials Chemistry* **2010**, 20(19), 3814–3826.
(34) Sharma, D. A Review of QR code Structure for Encryption and Decryption Process. *International Journal of Innovative Science and Research Technology* **2017**, 2(2), 13–18.
(35) Information capacity and versions of the QR Code (no date) Information capacity and versions of QR Code | QRcode.com | DENSO WAVE. Available at: https://www.qrcode.com/en/about/version.html.
(36) André, P. S., & Ferreira, R. A. S. Color Multiplexing of Quick-Response (QR) Codes. *Electronics Letters* **2014**, 50(24), 1828–1830.
(37) Lay, C. L., Koh, C. S. L., Wang, J., Lee, Y. H., Jiang, R., Yang, Y., Yang, Z., Phang, I. Y., Ling, X. Y. Aluminum Nanostructures with Strong Visible-Range SERS Activity for Versatile Micropatterning of Molecular Security Labels. *Nanoscale* **2018**, 10(2), 575-581

TOC

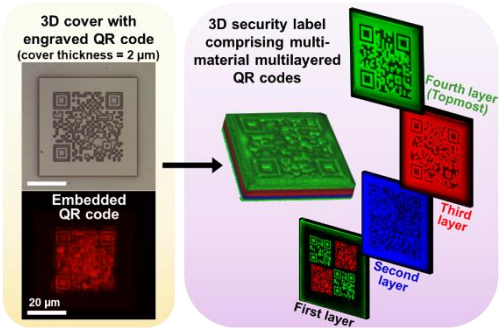

We achieve microfabrication of photostable perylene dye-incorporated security labels with multi-material, multilayered QR codes using two-photon lithography (TPL). An ultrathin 2.0 μm-thick 3D cover effectively conceals the embedded 2D QR codes, enhancing their security, leading us to successfully fabricate photostable multi-material QR code-based 3D security labels that possess enhanced data capacity by ≥ 5-fold and ensure data concealment.